JEE Journal of Ecological Engineering

Journal of Ecological Engineering 2024, 25(7), 137–150
https://doi.org/10.12911/22998993/187956
ISSN 2299–8993, License CC-BY 4.0

Received: 2024.03.21
Accepted: 2024.05.14
Published: 2024.06.01

Valorization of Iron Ore Tailings from Nador, Morocco, as a Sustainable Additive in the Manufacture of Red Clay Fired Bricks

Faiçal El Khazanti[1], Ahmed Rachid[1], Meriam El Ouahabi[2], Hicham Nasri[3], Dounia Azerkane[4], Yassine Et-Tayea[1], El Khadir Gharibi[2*]

[1] Laboratory Physico-Chemistry of Processes and Materials (PCPM), Research Team: Geology of Mining and Energy Resources (GRME), Hassan First University, Faculty of Sciences and Technology, 26002, Settat, Morocco

[2] UR. Art, Archaeology and Heritage (AAP), University of Liège, Belgium

[3] Applied Geosciences Laboratory, Faculty of Sciences, University Mohammed First, Mohammed V Avenue, Oujda, P.O. Box 60000, Morocco

[4] Laboratory of Applied Chemistry and Environment, Team of Mineral Solid Chemistry, Faculty of Sciences, Mohammed First University, Oujda 60000, Morocco

* Corresponding author's e-mail: gharibi_elkhadir@yahoo.fr

ABSTRACT

High iron ore production generates substantial solid waste. Storing this waste in dams poses environmental issues and safety risks for the population. The aim of this study was to valorize sterile waste (IOT) from an inactive iron mine in the Nador region of northeastern Morocco, as an additive in the manufacture of fired bricks made from a red clay (AJH) extracted from the Oujda region. For this purpose, brick specimens were obtained using a mix of a 40% of AJH and 60% of IOT. Physico-chemical, geotechnical and mineralogical characterization techniques were applied to qualify raw material. IOT consisted of hematite, magnetite, pyrite, jarosite and quartz and AJH of kaolinite, chlorite, calcite, hematite, dolomite, quartz and vermiculite. After firing the specimens at 500 °C, 850 °C and 1100 °C, mineralogical composition, bulk density, compressive strength and microstructure behavior of the specimens was assessed. The compressive strength of the bricks containing IOT is 1.25 MPa at T = 500 °C and it varies little at 1100 °C. The compressive strength of the reference sample is 2.94 MPa at 1100 °C. The material has low vitrification and greater porosity compared to the reference bricks. Adding IOT brings significant changes to the color of fired bricks.

Keywords: valorization, ferric mining waste, fired bricks, building, SEFERIF.

INTRODUCTION

Economic expansion has resulted in a rise in the consumption of minerals and metals. Consequently, mining activities, which are the primary source of these metals and minerals, have significantly increased (Ranängen and Lindman, 2017). However, this activity is accompanied by the production of more than 200 giga-tonnes from mining residues, such as sterile and slag (Valenta et al., 2023), their environmental and economic management constitutes a major challenge for companies and mining operators. To reduce environmental impacts and reuse mine tailings, several solutions have been proposed, depending on the nature of the ore and tailings.

Global production of iron and ferrous alloys amounts to 1.5 billion tonnes (Agboola et al., 2023), in 2010 it was accompanied by the production of 14 billion tonnes of residues (Islam and Murakami, 2021). The recycling and valorization of iron ore tailings (IOTs) is attracting interest in many areas, including the production of materials for the building and construction sector (Zhao et al., 2021; Xu et al., 2021; Singh et al., 2023; Moon et al., 2024). The integration of IOTs into construction materials like concrete, mortar, and paste has demonstrated the technical

viability of manufacturing products with suitable performance (Zhang et al., 2023; Li et al., 2023). IOTs were added to terracotta bricks (Zhang, 2013), particularly to study their impact on the firing temperature (Du et al., 2012). They were mixed with clay and other additives such as fly ash (Thejas et al., 2022; Cobîrzan et al., 2022) or sawdust ash (Elinwa et al., 2021). In Morocco, the presence of iron mineral deposits, notably the Beni Bou Ifrour massif (Nador province, north-east Morocco), has led to the development of significant mining activity. After its closure in 1976 (Bouabdellah et al., 2012), in the absence of appropriate rehabilitation measures, millions of tonnes of IOTs are exposed to climatic conditions, leading to the formation of acid mine drainage (AMD) (Khafouri et al., 2021).

Red clay exhibits refractory behavior during firing due to its high kaolinite content and the presence of gibbsite, which impedes sintering and creates pores in the material (Milheiro et al., 2005). Its optimal firing temperature must be above 950 °C, which accelerates sintering and the formation of the vitreous phase and provides better densification behavior (Mota et al., 2008). This study aimed to promote iron ore tailings from SEFERIF (Nador, north-eastern Morocco) in the production of fired construction bricks made from red clay. The objectives included investigating the impact of enriching red clays with iron oxide, derived from mining waste, on the firing temperature, mineralogy, and mechanical performance of the fired bricks. In addition to modifying the technological properties of red clay terracotta, this work also aimed to use IOT, rich in Fe_2O_3, as a pigment that dyes the ceramic clay a more intense red color. In this case, the bricks can be used in masonry and decoration of buildings.

MATERIAL AND METHODS

The samples used in this study, labeled IOT, were collected from different depths of the mining slag heaps at the SEFERIF iron mine. The red clay samples, labeled AJH, were sampled from the Triassic buttonhole of Jbel El Hamra and were used as a matrix for fired clay materials.

Geographical, historical and geological context of the iron mine

The Nador region in the eastern part of the Rif Oriental consists of Tertiary basins, tuffs, breccias, and volcanic rock flows (Kerchaoui, 1985). The Béni Bou Ifrour massif in northern Nador comprises slightly metamorphosed Jurassic and Cretaceous terrains intersected by Diorite veins and intrusions (El Bakkali et al., 1998; Roger et al., 2000; Duggen et al., 2005). Neogene tectonics influenced the evolution of the area, leading to sedimentation and emersion of the basins. The eastern part of the massif contains iron mineralization in its folded and metamorphosed Jurassic formations, divided into several deposits by tangential tectonics (Figure 1b) (Lebret., 2014).

The Nador SEFERIF iron mine consists of several deposits in the Beni Bou Ifrour massif: Ouixane (Wiksane or Ouichane), Axara-Imnassen and Bokoya-Setolazar (Figure 1a).

The deposits feature two types of mineralization: pyritic magnetite mineralization in fractures and as substitution in carbonate formations, and banded magnetite and pyrite mineralization in chlorite schists and tuffs with low iron content (Rhazi and Hayashi, 2002; Bouabdellah et al., 2016). From 1915 to its closure in 1976, the mines produced over 60 million tonnes of ore with iron contents between 45% and 60% (Bouabdellah et al., 2012). Of this, CEMR mined 24 million tonnes between 1915 and 1951 (Villand, 1966). The mine closure resulted in large volumes of waste rock and reserves estimated at over 35 million tonnes. Mineable resources are estimated at 26.4 million tonnes, with a grade of 57.5% iron and 4.02% sulfur (Bouabdellah et al., 2012; Khafouri et al., 2021).

Geological context of the red clays

The geology of Jbel Hamra (Mortier et al., 1967) begins with the Paleozoic outcrops at Jbel el Hamra, south of Oujda. This is succeeded by Red Triassic clays, Liassic age dolomitic limestones forming a deep aquifer, a substantial series of Miocene marls, Plio-Quaternary volcanic formations and, finally, Quaternary alluvial and lacustrine formations (Bengamra and Oujidi, 2015).

Analytical methods

At the Chemistry Department of the Oujda Faculty of Science, the following techniques are employed: Geotechnical characterization: particle size distribution by dry sieving (NF, 1997), sedimentometry (NF, 1992) and bulk density (EN, 1998).

- Spectrometric analysis: fourier transform infrared (FT/IR-4700, JASCO) in

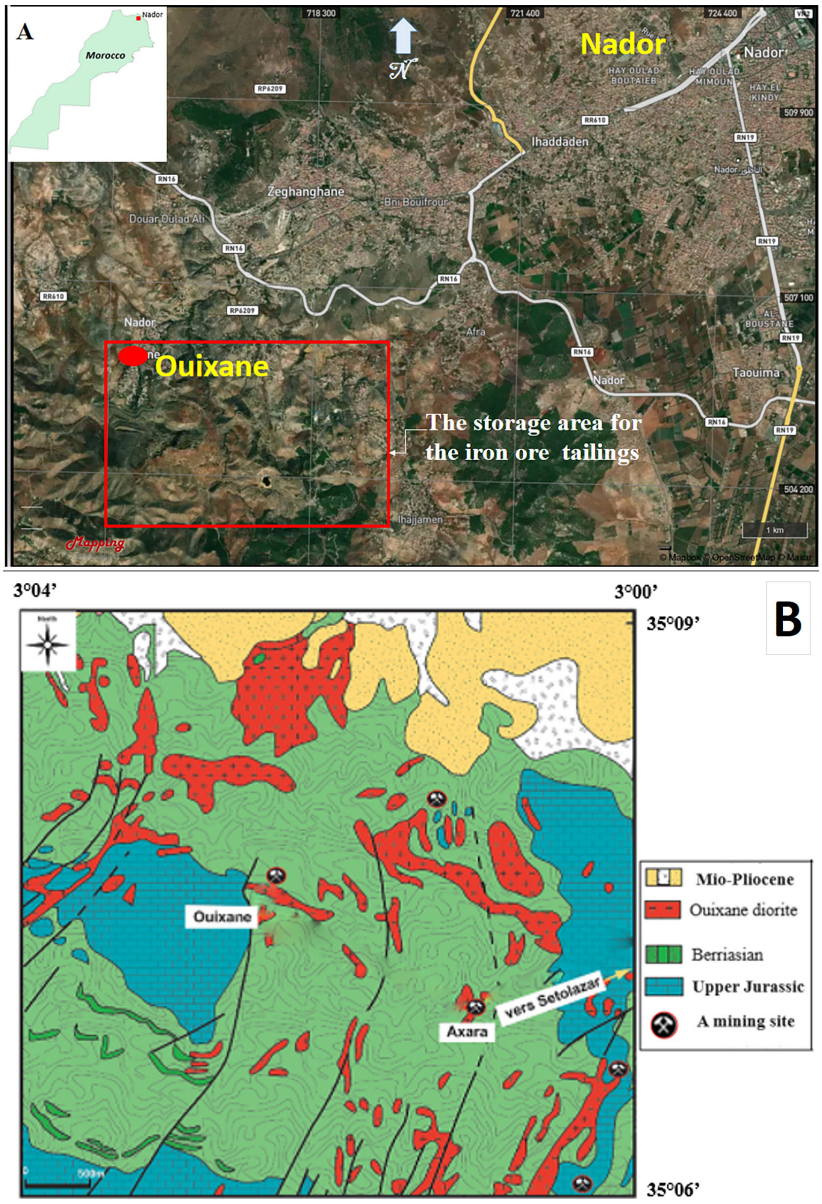

Figure 1. (a) Geographical location of SEFERIF's iron waste and mines, (b) geological map of the Beni Bou Ifrour massif (1/50000) (Lebret., 2014)

ATR (attenuated total reflectance) mode, equipped with a DLaTGS detector and Peltier temperature control. Measurements were taken at a frequency of 10 Hz with a resolution of 0.4 cm^{-1} in the wavelength range 400–4000 cm^{-1}.

- Thermal analysis: thermogravimetry (TGA/DTA) using the TGA/DTA Q500 and Q50 TA instrument (Shimadzu, Germany) at a temperature range from 20–900 °C and a heating rate of 10 °C/min.
- Mechanical characterization: resistance to mechanical compression was carried out using the TESTWELL device with a movement speed of 0.5 mm/min.
- The microstructure of raw materials was examined using a scanning electron microscope type (HIROX SH 5500 P, Europe Ltd., Japan). The elemental composition was also identified by an integrate energy dispersive spectroscopy (EDS, QUANTAX 100 Advanced, Bruker) operating in high vacuum, with an acceleration voltage of 10 kV. Additional techniques are conducted at the Faculty of Science and Technology of Settat, Hassan Premier University, Morocco.
- Chemical analysis by X-ray fluorescence using PANalytical Epsilon 3X.
- Mineralogical analysis by X-ray diffraction (XRD) using the D2 PHASER diffractometer,

equipped with a copper X-ray tube operating at 40 kV and 30 mA, in the range of 2°–70° 2θ.

Preparation of test specimens

Dried IOT mine waste and AJH clay samples were crushed, sieved (125 µm), and humidified. Two well-mixed samples were prepared: B-IOT (40% AJH, 60% IOT) and reference sample B-AJH (100% AJH clay). Both were mixed with distilled water (water/solid ratio = 0.45) and molded into cylindrical tubes (12 mm diameter, 24 mm height). After curing in stable humidity for 28 days, the specimens were oven-dried at 40 °C for 24 hours. The specimens were then annealed in a muffle furnace at temperatures ranging from 350 to 1100 °C, with a heating rate of 3 °C per minute and a 4-hour annealing period. Post heat treatment, the samples were left to cool in the oven. The fired specimens underwent mechanical compression tests and were characterized for their physical, mineralogical, and microstructural properties.

RESULTS AND DISCUSSION

Characterization of raw materials

Unground IOT materials from mine spoil heaps are characterized by an average particle size (D50) of around 800 µm, with a continuous spread curve indicating homogeneity between the particle size fractions in this sample. The shape of the curve is similar to that of material from a crushing process (Petlovanyi et al., 2021). The AJH clays mainly consist of clayey silts, with a clay content of 42%, a slightly higher silt content of 48% and 10% sand (Figure 2).

X-ray diffraction pattern (Figure 3) revealed that IOTs have a diverse iron-rich mineral phases, consisting of hematite (Fe_2O_3), magnetite (Fe_3O_4), pyrite (FeS_2) and jarosite $KFe_3(OH)_6(SO_4)_2$. The presence of different iron species reveals the geological and historical complexity of Nador's iron deposits (Walshe and Solomon, 1981). The presence of sulfur-rich geochemical conditions led to the formation of pyrite by intrusion-derived magmatic-hydrothermal fluids (Shawar et al., 2018). IOT waste also contains quartz (SiO_2) and anorthite ($CaAl_2Si_2O_8$), a plagioclase of magmatic origin. AJH clay mainly consists of clay mineral phases as kaolinite and chlorite and vermiculite. It also contains quartz, dolomite, calcite and hematite. Chemical composition, obtained by X-ray fluorescence (XRF) spectrometry (Table 1), reveals significant concentrations of iron (56.4% Fe_2O_3) and sulfur (13.9% SO_3) in IOT. They are rich in silicon (17.9% SiO_2). The AJH clay is highly rich in silicon (45.4% SiO_2), calcium (16.8% CaO), aluminum (12.6% Al_2O_3) and iron (10.6% Fe_2O_3). To compare the suitability of IOT and AJH as raw materials for the manufacture of fired bricks, ternary diagram SiO_2-Al_2O_3-(CaO+ MgO + Fe_2O_3 + K_2O) was plotted, drawn from the chemical analysis (Taha et al., 2016) (Figure 4). IOT mining waste is far from the realm of standard materials for the fired brick industry. It has low SiO_2 content compared to other reported IOTs used in construction materials (Young and Yang, 2019).

IOT infrared spectroscopy shows absorption bands at 358 cm^{-1}, 374 cm^{-1} and 450 cm^{-1}

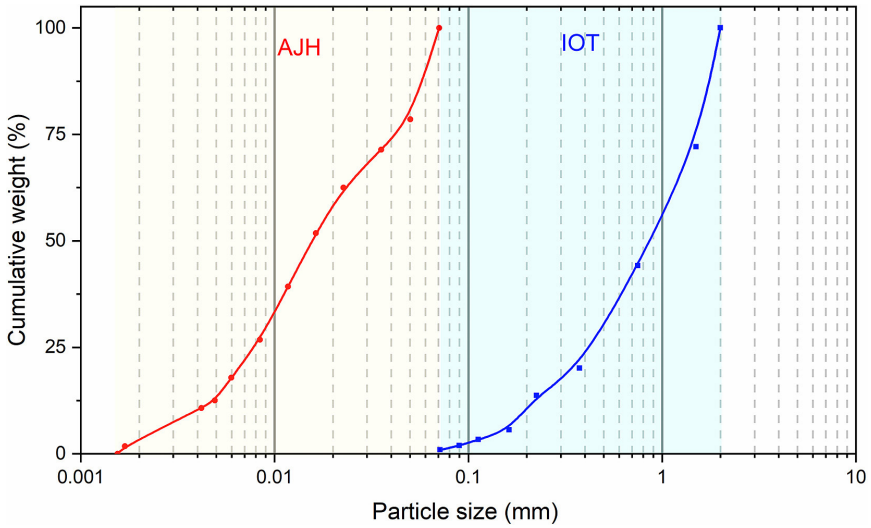

Figure 2. IOT and AJH particle size distribution

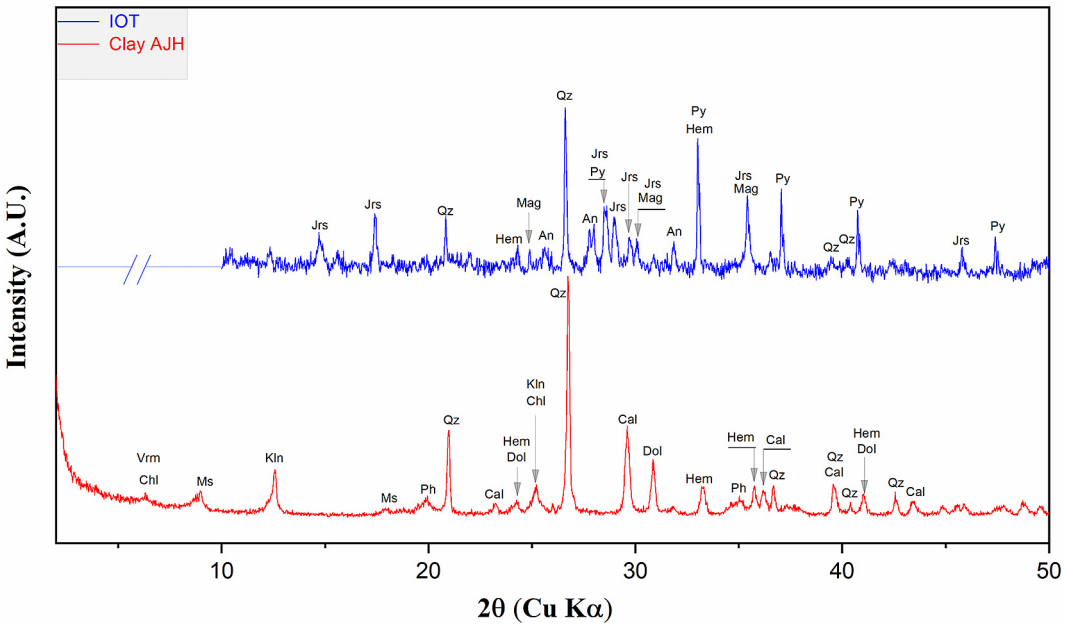

Figure 3. XRD patterns of IOT mining waste and AJH clay An: anorthite, Cal: calcite, Chl: chlorite, Dol: dolomite, Hem: hematite, Jrs: jarosite, Kln: kaolinite, Mag: magnetite, Ms: muscovite, Ph: phyllosilicates, Py: pyrite, Qz: quartz, Vrm: vermiculite

Table 1. Chemical composition of IOTs and AJH

Specification	IOT	AJH
Oxide	Mass (%)	
Fe_2O_3	56.4	10.6
SiO_2	17.9	45.4
SO_3	13.9	0.12
CaO	4.89	16.8
Al_2O_3	4.33	12.6
MgO	1.91	10.8
K_2O	0.64	1.72
P_2O_5	0.73	0.1
MnO	0.24	0.21
TiO_2	0.23	0.77
Ag_2O	0.1	–
Eu_2O_3	0.1	–
Cr_2O_3	–	0.01
Na_2O	–	0.32
SrO	–	0.04

attributed to the Fe-O bond of hematite and magnetite. Bands at 510, 596 and 625 cm^{-1} are linked to vibration modes specific to sulfide minerals such as pyrite (FeS_2). Similarly, the band at 794 cm^{-1} may correspond to the bending vibrations of the Fe-O-H bond in jarosite ($KFe_3(SO_4)_2(OH)_6$). The elongation vibration associated with ferric sulfates and ferrous sulfates gave bands at 1005 cm^{-1}, 1087 cm^{-1} and 1150 cm^{-1} (De Donato et al., 1999; Derycke et al., 2013). The bands around 445 cm^{-1} and 516 cm^{-1} characterize the deformation vibrations of the Si-O bond of quartz, and those at 1617 cm^{-1} and 3368 cm^{-1} are associated with the elongation and deformation vibration of the OH group of adsorbed water (De Donato et al., 1999) (Figure 5). The infrared spectrum of AJH shows a band at 358 cm^{-1} of the Fe-O bond of iron oxides, and two characteristic bands at 3562 cm^{-1} and 3400 cm^{-1}, corresponding to the vibrations of structural hydroxyl groups specific to kaolinite. The band at 1397 cm^{-1} is associated with the elongation and deformation vibration of the OH group of adsorbed water. The two bands at 976 cm^{-1} and 872 cm^{-1} are due to the elongation vibration of the Si-O-Si group in kaolinite or quartz. The absorption bands observed at 1978 cm^{-1}, 2048 cm^{-1} and 2161 cm^{-1} correspond to the vibration of carbonate bonds. The bands characteristic of deformation vibrations of the Si-O bond in quartz occurs around 445 cm^{-1}, 516 cm^{-1} and 672 cm^{-1}.

Thermal analysis of IOT mine wastes (Figure 6a) revealed an endothermic peak centered around 100 °C, with a mass loss of 1.4%, corresponding to moisture water loss. Two further endothermic peaks appear at 497 °C and 530 °C, with mass losses of 10% and 13%, respectively, corresponding to the oxidation of pyrite (Nakamura et al., 1994; Aracena and Jerez, 2021). Thermal analysis of AJH clay, previously dried, revealed slight endothermic

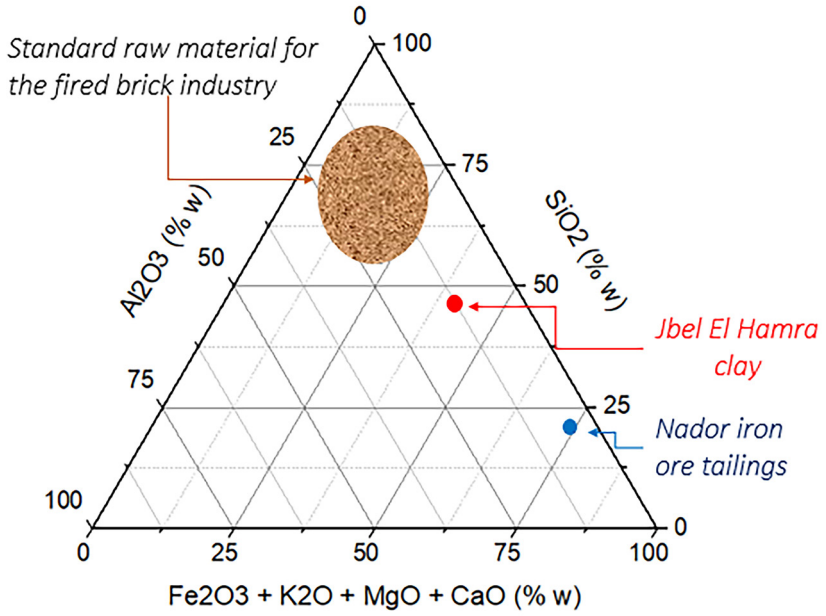

Figure 4. Position of IOTs and AJH on ternary diagram SiO_2-$Al2O_3$-(CaO + MgO + Fe_2O_3 + K_2O)

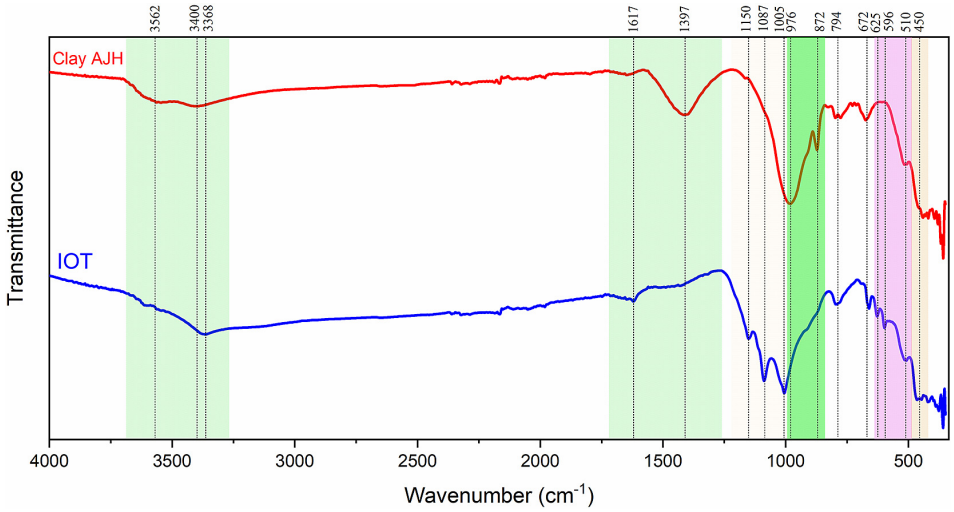

Figure 5. Infrared spectroscopy of IOT and AJH

dehydration at 68 °C, with a mass loss of around 1%. The endothermic peak appears at 564 °C, with a mass loss of around 4%, corresponding to the dehydroxylation of kaolinite, and the intense, broad endothermic peak, centered at 750 °C, characteristic of calcite decarbonation. It is associated with a 15% weight loss (Figure 6b).

Characterization of fired bricks

Physical properties

Figure 7a shows that the apparent densities of the fired bricks decrease as a function of the firing temperature. Before firing, the B-AJH and B-IOT specimens, and after 28 days of setting, had apparent densities equal to 334 kg·m^{-3} and 498 kg·m^{-3} respectively. The density of B-IOT, rich in ferrous compounds, is higher than that of B-AJH. When B-AJH is fired between 500 °C and 1100 °C its density decreases by 22.7%, it goes from 310 kg·m^{-3} to 223 kg·m^{-3} while the rate of reduction in densities of the B-IOT specimens, is 15.2%. It decreases from 486 kg·m^{-3} to 413 kg·m^{-3}. The evolution of specimen weight loss during firing is shown in figure 7b. Losses from B-AJH, which is rich in clays and carbonates that decompose at high temperatures, are greater than those from B-IOT.

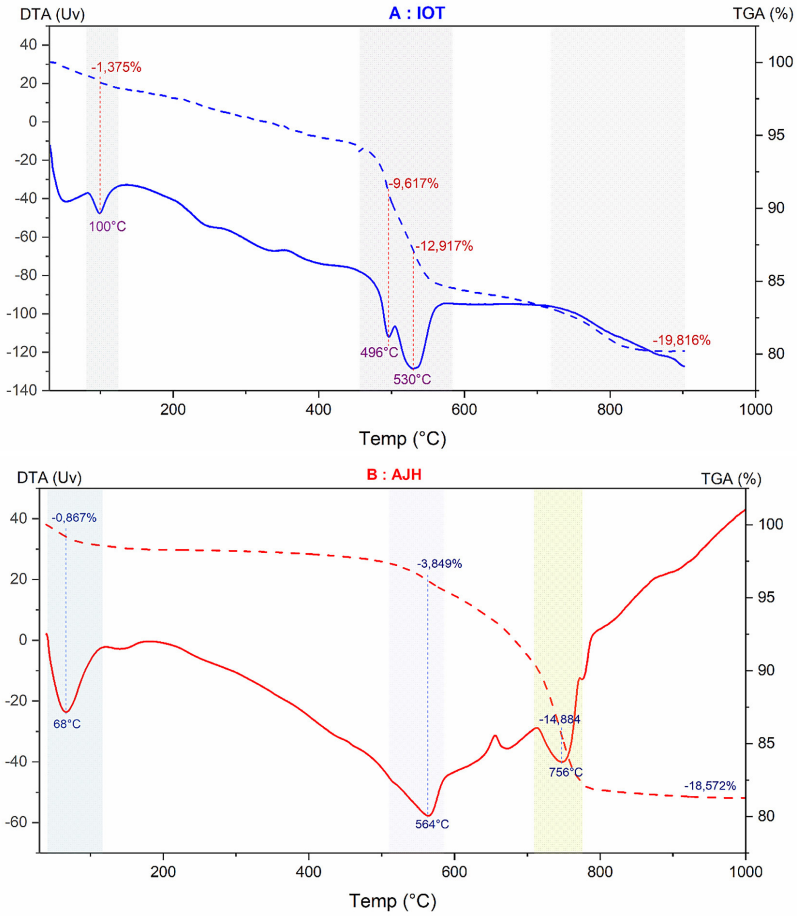

Figure 6. Thermogravimetric analysis of (a) IOT and (b) AJH

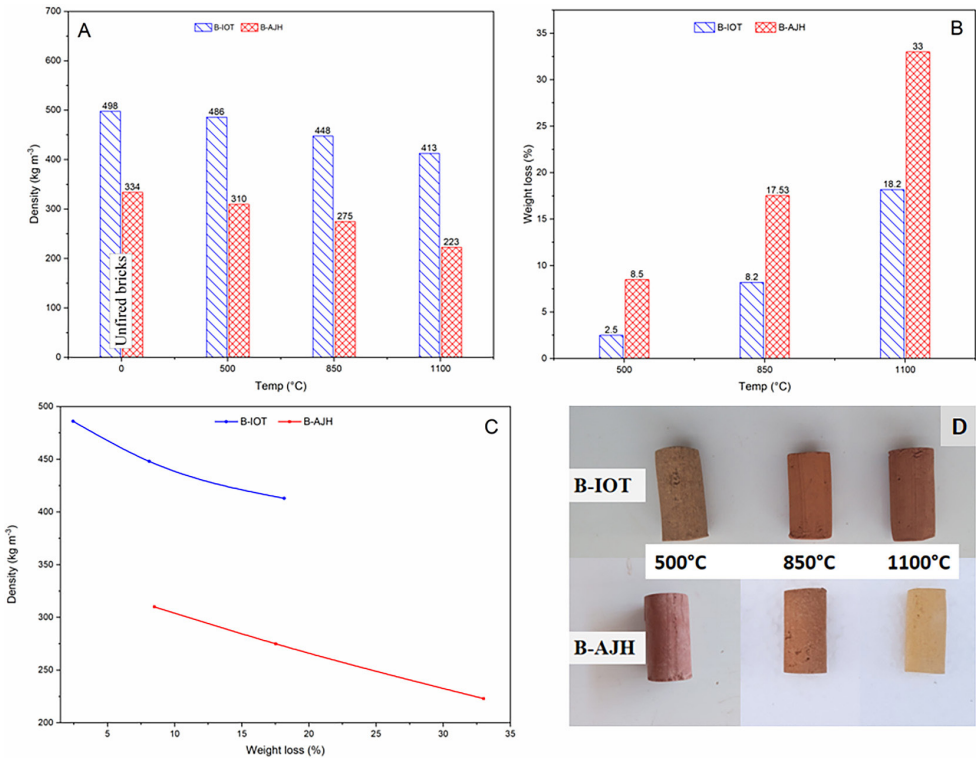

Figure 7. (a) variation in density, (b) weight loss of B-IOT and B- AJH as a function of firing temperature, (c) weight loss evolution of B-IOT and B- AJH in term of density evolution, (d) appearance of the fired specimens

The loss of mass is associated with the departure of volatile compounds, causing the expansion of materials and potentially reducing density (Weng et al., 2003; Moujoud et al., 2023). Figure 7c clearly shows an almost linear decrease in density as a function of mass loss.

As regards the color of fired specimens, B-AJH goes from light red at 500 °C to yellow at 1100 °C, while B-IOT specimens change from greenish red to dark red (Figure 7d). Fe_2O_3 acts as a pigment that dyes the clay fired with a more intense red color (Monteiro and Vieira, 2014; Adamou et al., 2023).

Compressive strength

Figure 8 shows that mechanical compressive strength increases along with the firing temperature. For B-AJH reference specimen, the increase is 203%, with compressive strength rising from 0.97 MPa at 500 °C to 2.94 MPa at 1100 °C. For B-IOT specimens, the increase is slight, amounting to 35.8%. The improved mechanical performance of specimens as a function of firing temperature is attributed to the increased vitrification of clay materials. This vitrification strengthens the bonds between clay particles and improves the mechanical resistance of fired bricks (Phonphuak and Chindaprasirt, 2015).

Vitrification of clay bricks results in higher density, less water absorption and lower drying shrinkage (Phonphuak et al., 2016). During clay firing, at T > 750 °C, hematite nucleates and grows in specific micro-domains (Nodari et al., 2007) and the presence of large amounts of iron oxide can reduce the firing temperature and vitrification range (Sarkar et al., 2010). The poor mechanical performance of B-IOT could be explained by hematite nucleation and low vitrification of the fired material.

Mineralogical composition

Mineralogical composition of fired specimens shows that, depending on firing temperature, some phases of the raw material disappear and other mineral phases appear (Figure 9).

In the case of B-AJH (Figure 9a), at low temperature (T = 350 °C), the phases present in the clay were unchanged. However, at high temperatures (T > 700 °C), several transformations take place. Clay mineral phases and carbonate minerals (calcite and dolomite) disappear, giving way to other neoformed phases such as silicate minerals like gehlenite ($Ca_2Al[AlSiO_7]$), belonging to the melilite group (Bauluz et al., 2004), wollastonite ($CaSiO_3$), diopside ($CaMgSi_2O_6$), enstatite ($Mg_2Si_2O_6$) and anorthite ($CaAl_2Si_2O_8$). The newly formed phases come from the reaction of lime, resulting from the decomposition of carbonates (calcite and dolomite), with the oxides produced by the decomposition of the clay phases (Trindade et al., 2009; El Ouahabi et al., 2015). At T = 1100 °C, anhydrite disappears; in the presence of quartz, anhydrite can decompose at

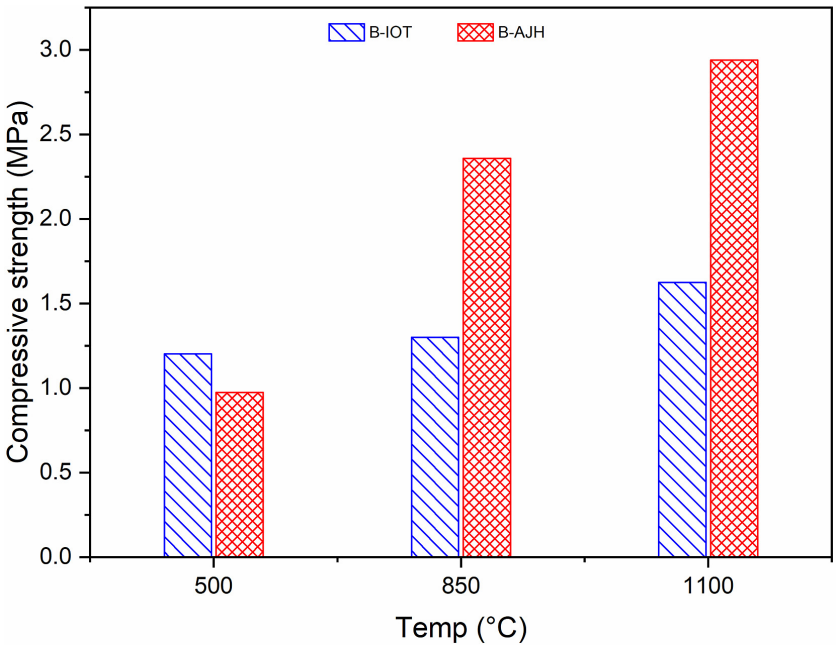

Figure 8. Compressive strength as a function of firing temperature

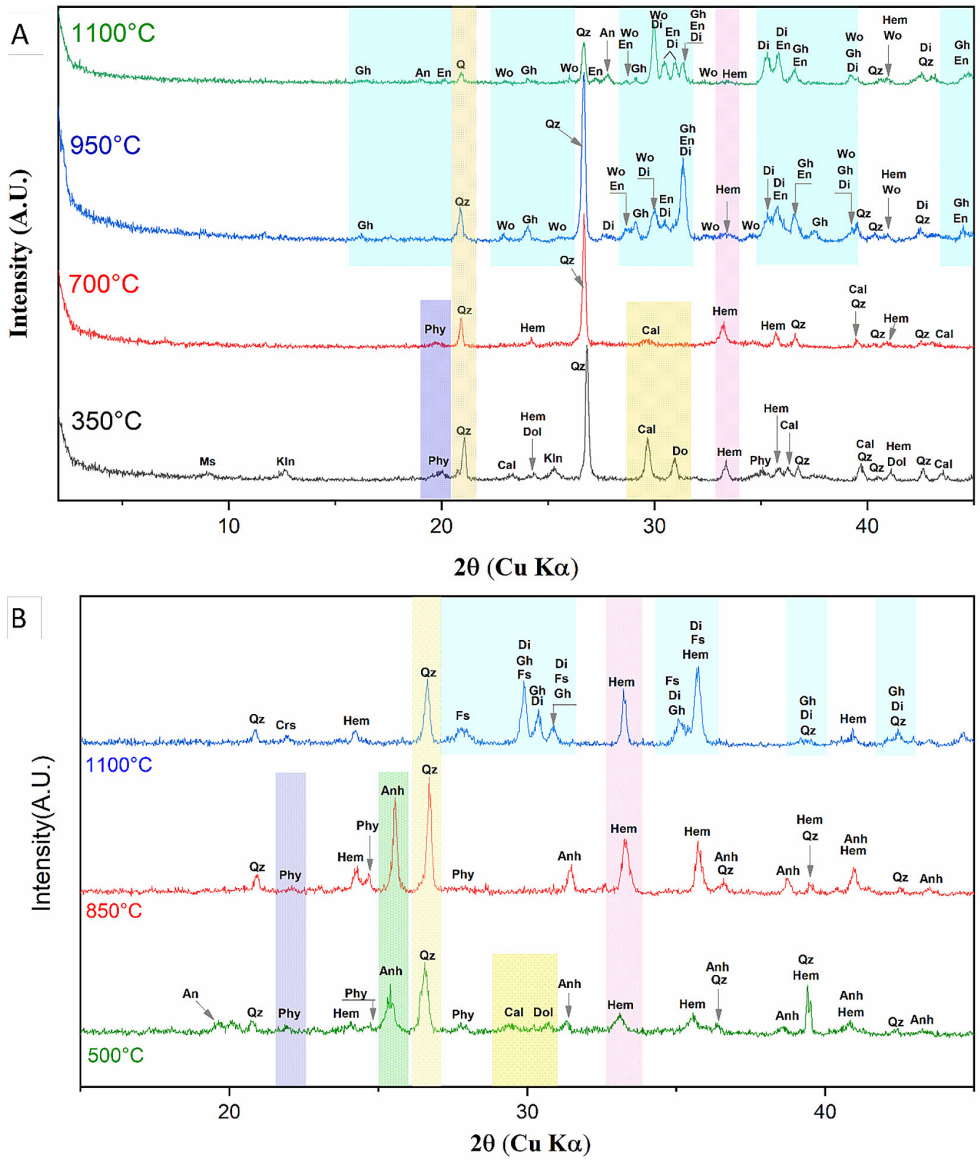

Figure 9. XRD patterns of (a) B-AJH and (b) B-IOT fired bricks – An: anorthite, Anh: anhydrite, Cal: calcite, Crs: cristobalite, Di: diopside, Dol: dolomite, En: enstatite, Fs: ferrosilite, Gh: gehlenite, Hem: hematite, Kln: kolinite, Ms: muscovite, Phy: phyllosilicates, Qz: quartz, Wo: wollastonite

1000 °C to form wollastonite (Cultrone and Rosua, 2020) (Equation 1).

$$CaSO_4 + SiO_2 \rightarrow CaSiO_3 + SO_3(g) \quad (1)$$

Quartz and hematite, present in AJH, persist throughout the heat treatment. The amount of quartz decreases with increasing firing temperature. Quartz decomposes gradually from 800 to 1100 °C, diminishing drastically at 1100 °C (Trindade et al., 2009). For B-IOT (Figure 9b), at 500 °C, pyrite, magnetite and jarosite disappear and anhydrite and diopside appear. However, at high firing temperatures, especially at 1100 °C, the last two phases disappear and cristobalite as well as ferrosilite appear. Quartz and hematite are present in all firing temperatures. Cristobalite may crystallize from quartz (Pardo et al., 2011; Jusnes et al., 2021). At high (T > 900 °C) and very low temperatures, and almost constant oxygen fugacity, ferrosilite can crystallize (Laita et al., 2019) through FeS-SiO_2 interaction (Bataleva et al., 2017). Wollastonite does not appear in the B-IOT sample, probably because the amount of calcium in IOT is not sufficient to give a quantity of wollastonite detectable by XRD. The disappearance of pyrite at low temperatures can be interpreted as its oxidation and transformation into hematite (Nakamura et al., 1994; Aracena and Jerez, 2021) (Equation 2). The disappearance of jarosite ($KFe_3(SO_4)_2(OH)_6$) in the specimen kilned at 500 °C can be attributed to its conversion into hematite (He

et al., 2023). As for the disappearance of magnetite, it can be explained by its oxidation into hematite (Ponomar et al., 2020) (Equation 3). The formation of anhydrite can be attributed to the interaction between calcium-rich minerals (such as calcite and dolomite) and sulfide gases, which are a result of the decomposition of sulfide minerals (like pyrite) (Taha et al., 2016).

$$2FeS_2 + 5.5O_2 \rightarrow Fe_2O_3 + 4SO_2 \quad (2)$$

$$4Fe_3O_4 + O_2 \rightarrow 6Fe_2O_3 \quad (3)$$

Microstructure by SEM images

Figure 10 gives the morphological appearance of the reference specimen B-AJH. At low temperatures (T = 500 °C), they exhibit low porosity and vitrification. This low-temperature vitrification behavior of red clay has been widely used by the ceramics industry for the production of ceramic floor and wall tiles (Dana et al., 2023). The vitrification of specimens decreases at high temperatures, while porosity increases (T = 1100 °C).

The addition of IOT waste modified the microstructure of the specimens, leading to a reduction in vitrification which prevented porosity filling (Figure 11). At low temperatures (T = 500 °C), micropores appear in the material and there is no trace of vitrification. At T = 1100 °C, the pores become larger and glassy zones appear on the sample. High porosity gives B-IOT low

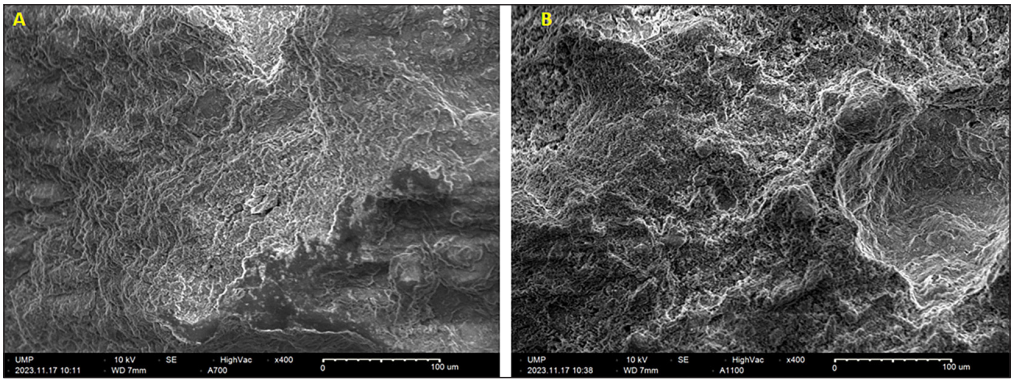

Figure 10. SEM images of B-AJH specimens fired at 500 °C (a) and 1100 °C (b)

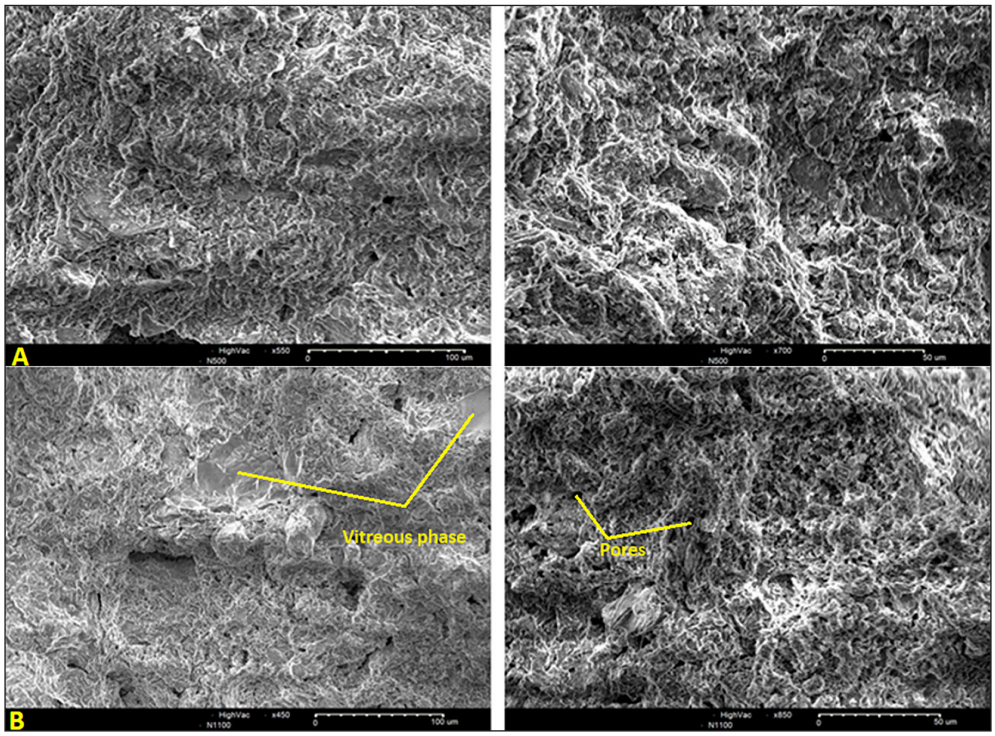

Figure 11. SEM images of B-IOT specimens fired at 500 °C (a) and 1100 °C (b)

thermal conductivity, making it an excellent insulator (Crespo-López et al., 2024).

The growth in compressive strength of B-IOT between 500 and 1100 °C was low (Figure 8), as there was compensation between two opposing phenomena: on the one hand, the increase in porosity which reduced compressive strength, and on the other, the appearance of partial vitrification which increased compressive strength (Liu at al., 2019).

CONCLUSIONS

Mining waste (IOT) from the inactive iron mine in Nador (north-east Morocco) is rich in iron oxides and sulfides, mainly hematite (Fe_2O_3), magnetite (Fe_3O_4) and pyrite (FeS_2), with an average particle size of around 800 µm. Following the mine closure, these were deposited in dam-like structures, leading to numerous issues, particularly environmental ones. The valorization of Nador's IOT in the manufacture of red earth bricks is very promising.

- Upon concluding this work, which aimed to promote the use of Nador's IOT in the production of fired red clay bricks, it can be deduced that the addition of IOT to red clay reduces the compressive strength of fired bricks, which increases slightly depending on the temperature, comparable to the control brick.
- The addition of IOT results in significant changes in the color of red clay fired bricks. The color change, which evolves towards dark red, depends on the firing temperature. B-IOT bricks can be used for the decoration of buildings and other structures
- The incorporation of IOT reduces the decreases the vitrification of red clay terracotta, which do not fill the pores that form during the firing of clays.
- The losses on ignition of the specimens containing IOT are lower than those containing only red clay.

REFERENCES

1. Adamou, J.M.K., Ntouala, R.F.D., Effoudou, E.N., Bineli, M.T.N., Ze, A.N.O., Hamadjida, G., Onana, V.L. 2023. Mineralogical, geochemical, and geotechnical features of lateritic soils from termite mounds in two contrasting savannah areas (central Cameroon) as raw materials for brick making. Heliyon, 9(6). https://doi.org/10.1016/j.heliyon.2023.e17257
2. Agboola, O., Babatunde, D.E., Fayomi, O.S.I., Sadiku, E.R., Popoola, P., Moropeng, L., Yahaya A., Mamudu, O.A. 2020. A review on the impact of mining operation: Monitoring, assessment and management. Results in Engineering, 8, 100181. https://doi.org/10.1016/j.rineng.2020.100181
3. Aracena, A., Jerez, O. 2021. Mechanism and kinetics of pyrite transformation at elevated temperatures. Physicochemical Problems of Mineral Processing, 57. http://dx.doi.org/10.37190/ppmp/143124
4. Bataleva, Y.V., Palyanov, Y.N., Borzdov, Y.M., Bayukov, O.A., Zdrokov, E.V. 2017. Iron carbide as a source of carbon for graphite and diamond formation under lithospheric mantle PT parameters. Lithos, 286, 151–161. https://doi.org/10.1016/j.lithos.2017.06.010
5. Bauluz, B., Mayayo, M.J., Yuste, A., Fernandez-Nieto, C., Lopez, J.G. 2004. TEM study of mineral transformations in fired carbonated clays: relevance to brick making. Clay Minerals, 39(3), 333–344. https://doi.org/10.1180/0009855043930138
6. Bengamra, S., Oujidi, M. 2015. Mineralogy of atmospheric dust deposits in the Naima-El Aioun basin (Eastern Morocco). J. Mater. Environ. Sci. 6(8) 2076–2082
7. Bouabdellah, M., Jabrane, R., Margoum, D., Sadequi, M. 2016. Skarn to porphyry-epithermal transition in the Ouixane Fe District, Northeast Morocco: interplay of meteoric water and magmatic-hydrothermal fluids. Mineral Deposits of North Africa, 201–225. https://doi.org/10.1007/978-3-319-31733-5_7
8. Bouabdellah, M., Lebret, N., Marcoux, E., Sadequi, M. 2012. Les mines des Beni Bou Ifrour-Ouixane (Rif Oriental): un district ferrugineux néogène de type skarns The Beni Bou Ifrour-Ouixane mines (Eastern Rif), Neogene Skarn Type Iron Deposits. Nouveaux Guides Géologiques et miniers du Maroc, 357–362.
9. Cobîrzan, N., Muntean, R., Thalmaier, G., Felseghi, R.A. 2022. Recycling of mining waste in the production of masonry units. Materials, 15(2), 594. https://doi.org/10.3390/ma15020594
10. Crespo-López, L., Coletti, C., Arizzi, A., Cultrone, G. 2024. Effects of using tea waste as an additive in the production of solid bricks in terms of their porosity, thermal conductivity, strength and durability. Sustainable Materials and Technologies, 39, e00859. https://doi.org/10.1016/j.jmrt.2023.03.189
11. Cultrone, G., Rosua, F. J. C. 2020. Growth of metastable phases during brick firing: Mineralogical and microtextural changes induced by the composition of the raw material and the presence of additives. Applied Clay Science, 185, 105419. https://doi.org/10.1016/j.clay.2019.105419
12. Dana, K., Rakib, S.A., Sinhamahapatra, S. 2023.

Effect of oxide additives on densification of terracotta. Applied Clay Science, 245, 107147. https://doi.org/10.1016/j.clay.2023.107147

13. De Donato, P., Kongolo, M., Barres, O., Yvon, J., Enderle, F., Bouquet, E., Alnot M., Cases, J.M. 1999. Chemical surface modifications of sulphide minerals after comminution. Powder Technology, 105(1–3), 141-148. https://doi.org/10.1016/S0032-5910(99)00129-1
14. Derycke, V., Kongolo, M., Benzaazoua, M., Mallet, M., Barrès, O., De Donato, P., Bussière B., Mermillod-Blondin, R. 2013. Surface chemical characterization of different pyrite size fractions for flotation purposes. International Journal of Mineral Processing, 118, 1–14. https://doi.org/10.1016/j.minpro.2012.10.004
15. Du, G.X., Zuo, R.F., Guo, W.J., Liao, J.H. 2012. Preparation of construction bricks from iron ore tailings. Advanced Materials Research, 557, 839–844. https://doi.org/10.4028/www.scientific.net/AMR.557-559.839
16. Duggen, S., Hoernle, K., van den Bogaard, P., Garbe-Schönberg, D. 2005. Post-collisional transition from subduction-to intraplate-type magmatism in the westernmost Mediterranean: evidence for continental-edge delamination of subcontinental lithosphere. Journal of Petrology, 46(6), 1155–1201. https://doi.org/10.1093/petrology/egi013
17. El Bakkali, S., Gourgaud, A., Bourdier, J.L., Bellon, H., Gundogdu, N. 1998. Post-collision neogene volcanism of the Eastern Rif (Morocco): magmatic evolution through time. Lithos, 45(1–4), 523–543. https://doi.org/10.1016/S0024-4937(98)00048-6
18. El Ouahabi, M., Daoudi, L., Hatert, F., Fagel, N. 2015. Modified mineral phases during clay ceramic firing. Clays and Clay Minerals, 63(5), 404–413. https://doi.org/10.1346/CCMN.2015.0630506
19. Elinwa, A. U., Mohammed, A. S., Mohammed, A. B. 2021. Effects of the Addition of Sawdust Ash and Iron Ore Tailings on the Characteristics of Clay Soil. Journal of Building Material Science, 3(2), 27–38. https://doi.org/10.30564/jbms.v3i2.3732
20. EN 1998. EN. B.1097-3. Tests for mechanical and physical properties of aggregates. Determination of loose bulk density and voids, British Standards Institution.
21. He, D., Jiang, F., Fu, X., Liu, R., Han, H., Sun, W., Niu, Z., Yue, T. 2023. Recycling of hazardous jarosite residues based on hydrothermal crystal transformation. Waste Management, 172, 290–298. https://doi.org/10.1016/j.wasman.2023.10.026
22. Islam, K., Murakami, S. 2021. Global-scale impact analysis of mine tailings dam failures: 1915–2020. Global Environmental Change, 70, 102361. https://doi.org/10.1016/j.gloenvcha.2021.102361
23. Jusnes, K.F., Tangstad, M., Ringdalen, E. 2021. Phase transformations in quartz used in silicon and ferrosilicon. Aspects in Mining & Mineral Science 5(5). http://dx.doi.org/10.31031/AMMS.2020.05.000622
24. Kerchaoui, S. 1985. Etude géologique et structurale du massif des Beni Bou Ifrour (Rif oriental, Maroc) (Doctoral dissertation, Paris 11) (in frensh).
25. Khafouri, A., Talbi, E. H., Abdelouas, A. 2021. Assessment of heavy metal contamination of the environment in the mining site of Ouixane (North East Morocco). Water, Air, & Soil Pollution, 232(10), 398. https://doi.org/10.1007/s11270-021-05318-6
26. Laita, E., Bauluz, B., Yuste, A. 2019. High-temperature mineral phases generated in natural clinkers by spontaneous combustion of coal. Minerals, 9(4), 213. https://doi.org/10.3390/min9040213
27. Lebret, N. 2014. Contexte structural et métallogénique des skarns à magnétite des Beni Bou Ifrour (Rif oriental, Maroc) Apports à l'évolution géodynamique de la Méditerranée occidentale (Doctoral dissertation, Université d'Orléans).
28. Li, Y., Liu, L., Deng, Y., Chen, Y., Li, Y., Wu, J. 2023. Unlocking the potential of iron ore tailings in controlled low-strength material: Feasibility, performance, and evaluation. Journal of Cleaner Production, 423, 138772. https://doi.org/10.1016/j.jclepro.2023.138772
29. Liu, T., Lin, C., Liu, P., Liu, J., Li, C., Han, L., Zhou, X., Yang, Q., Lu, A. 2019. Preparation and characterization of partially vitrified ceramic material. Journal of Non-Crystalline Solids, 505, 92–101. https://doi.org/10.1016/j.jnoncrysol.2018.10.019
30. Milheiro, F.A.C., Freire, M.N., Silva, A.D., Holanda, J.N.F. 2005. Densification behaviour of a red firing Brazilian kaolinitic clay. Ceramics International, 31(5), 757–763. https://doi.org/10.1016/j.ceramint.2004.08.010
31. Monteiro, S.N., Vieira, C.M.F. 2014. On the production of fired clay bricks from waste materials: A critical update. Construction and Building Materials, 68, 599–610. https://doi.org/10.1016/j.conbuildmat.2014.07.006
32. Moon, S., Kim, E., Noh, S., Triwigati, P.T., Choi, S., Park, Y. 2024. Carbon Mineralization of Steel and Iron-Making Slag: Paving the Way for a Sustainable and Carbon-Neutral Future. Journal of Environmental Chemical Engineering, 112448. https://doi.org/10.1016/j.jece.2024.112448
33. Mortier, F., Quang, N., Sadek, M. 1967. Hydrogéologie des formations volcaniques du nord-est du Maroc. Service des Ressources en Eau de l'Office National des Irrigations du Maroc, 327–333.
34. Mota, L., Toledo, R., Machado, F.A.L., Holanda, J. N.F., Vargas, H., Faria Jr, R.T. 2008. Thermal characterisation of red clay from the Northern Region of Rio de Janeiro State, Brazil using an open

photoacoustic cell, in relation to structural changes on firing. Applied Clay Science, 42(1–2), 168–174. https://doi.org/10.1016/j.clay.2008.01.010

35. Moujoud, Z., Harrati, A., Manni, A., Naim, A., El Bouari, A., Tanane, O. 2023. Study of fired clay bricks with coconut shell waste as a renewable pore-forming agent: Technological, mechanical, and thermal properties. Journal of Building Engineering, 68, 106107. https://doi.org/10.1016/j.jobe.2023.106107
36. Nakamura, H., Sato, S., Hara, Y. 1994. The oxidation of pyrite. Journal of hazardous materials, 37(2), 253–263. https://doi.org/10.1016/0304-3894(93)E0095-J
37. NF, 1992. NF. P. 94-057-Analyse granulométrique des sols-Méthode par sédimentation. Norme Française, AFNOR, Paris.
38. NF, (1997). NF EN 933-1., 1997. Essais pour déterminer les caractéristiques géométriques des granulats, Partie 1 : Détermination de la granularité Analyse granulométrique par tamisage, AFNOR, Paris
39. Nodari, L., Marcuz, E., Maritan, L., Mazzoli, C., Russo, U. 2007. Hematite nucleation and growth in the firing of carbonate-rich clay for pottery production. Journal of the European Ceramic Society, 27(16), 4665–4673. https://doi.org/10.1016/j.jeurceramsoc.2007.03.031
40. Pardo, F., Meseguer, S., Jordán, M.M., Sanfeliu, T., González, I. 2011. Firing transformations of Chilean clays for the manufacture of ceramic tile bodies. Applied Clay Science, 51(1–2), 147–150. https://doi.org/10.1016/j.clay.2010.11.022
41. Petlovanyi, M., Malashkevych, D., Sai, K., Bulat, I., Popovych, V. 2021. Granulometric composition research of mine rocks as a material for backfilling the mined-out area in coal mines. Mining of Mineral Deposits. 15(4), 122–129. http://ir.nmu.org.ua/handle/123456789/160814
42. Phonphuak, N., Chindaprasirt, P. 2015. Types of waste, properties, and durability of pore-forming waste-based fired masonry bricks. Eco-efficient masonry bricks and blocks, 103–127. https://doi.org/10.1016/B978-1-78242-305-8.00006-1
43. Phonphuak, N., Kanyakam, S., Chindaprasirt, P. 2016. Utilization of waste glass to enhance physical–mechanical properties of fired clay brick. Journal of Cleaner production, 112, 3057–3062. https://doi.org/10.1016/j.jclepro.2015.10.084
44. Ponomar, V.P., Bagmut, M.M., Kalinichenko, E. A., Brik, A. B. 2020. Experimental study on oxidation of synthetic and natural magnetites monitored by magnetic measurements. Journal of Alloys and Compounds, 848, 156374. https://doi.org/10.1016/j.jallcom.2020.156374
45. Ranängen, H., Lindman, Å. 2017. A path towards sustainability for the Nordic mining industry. Journal of Cleaner Production, 151, 43–52. https://doi.org/10.1016/j.jclepro.2017.03.047
46. Rhazi, M.E., Hayashi, K.I. 2002. Mineralogy, geochemistry, and age constraints on the Beni Bou Ifrour skarn type magnetite deposit, northeastern Morocco. Resource Geology, 52(1), 25–39. https://doi.org/10.1111/j.1751-3928.2002.tb00114.x
47. Roger, S., Münch, P., Cornée, J. J., Saint Martin, J.P., Féraud, G., Pestrea, S., Conesa G., Moussa, A.B. 2000. 40Ar/39Ar dating of the pre-evaporitic Messinian marine sequences of the Melilla basin (Morocco): a proposal for some biosedimentary events as isochrons around the Alboran Sea. Earth and Planetary Science Letters, 179(1), 101–113. https://doi.org/10.1016/S0012-821X(00)00094-7
48. Sarkar, R., Singh, N., Das Kumar, S. 2010. Utilization of steel melting electric arc furnace slag for development of vitreous ceramic tiles. Bulletin of Materials Science, 33, 293–298. https://doi.org/10.1007/s12034-010-0045-5
49. Shawar, L., Halevy, I., Said-Ahmad, W., Feinstein, S., Boyko, V., Kamyshny, A., Amrani, A. 2018. Dynamics of pyrite formation and organic matter sulfurization in organic-rich carbonate sediments. Geochimica et Cosmochimica Acta, 241, 219–239. https://doi.org/10.1016/j.oregeorev.2016.09.002
50. Singh, D., Kumar, R., Nighot, N.S., Rajput, A., Prajapati, A., Singh, B.K., Kirgiz, M.S., Srinivasaraonaik, B., Khans, S., Mishra, R.K., Lakhani, R. 2023. A comprehensive review on valorisation of octal by-product as supplementary admixtures in the production of fired and unfired bricks. Construction and Building Materials, 408, 133641. https://doi.org/10.1016/j.conbuildmat.2023.133641
51. Taha, Y., Benzaazoua, M., Mansori, M., Yvon, J., Kanari, N., Hakkou, R. 2016. Manufacturing of ceramic products using calamine hydrometallurgical processing wastes. Journal of Cleaner Production, 127, 500–510. https://doi.org/10.1016/j.jclepro.2016.04.056
52. Thejas, H.K., Hossiney, N. 2022. Alkali-activated bricks made with mining waste iron ore tailings. Case Studies in Construction Materials, 16, e00973. https://doi.org/10.1016/j.cscm.2022.e00973
53. Trindade, M.J., Dias, M.I., Coroado, J., Rocha, F. 2009. Mineralogical transformations of calcareous rich clays with firing: A comparative study between calcite and dolomite rich clays from Algarve, Portugal. Applied Clay Science, 42(3–4), 345–355. https://doi.org/10.1016/j.clay.2008.02.008
54. Valenta, R.K., Lèbre, É., Antonio, C., Franks, D. M., Jokovic, V., Micklethwaite, S., Parbhakar-Fox, A., Runge, K., Savinova, E., Segura-Salazar, J., Stringer, M., Verster, I., Yahyaei, M. 2023. Decarbonisation to drive dramatic increase in mining waste–Options for reduction. Resources, Conservation and Recycling, 190, 106859. https://doi.org/10.1016/j.resconrec.2022.106859

55. Villand, J. C. 1966. Etude pétrographique dans le Beni Bou Ifrour, Maroc Nord oriental. Rapport Note, BRPM, 24.
56. Walshe, J.L., Solomon, M. 1981. An investigation into the environment of formation of the volcanic-hosted Mt. Lyell copper deposits using geology, mineralogy, stable isotopes, and a six-component chlorite solid solution model. Economic Geology, 76(2), 246–284. https://doi.org/10.2113/gsecongeo.76.2.246
57. Weng, C. H., Lin, D. F., Chiang, P. C. 2003. Utilization of sludge as brick materials. Advances in environmental research, 7(3), 679–685. https://doi.org/10.1016/S1093-0191(02)00037-0
58. Xu, F., Wang, S., Li, T., Liu, B., Li, B., Zhou, Y. 2021. Mechanical properties and pore structure of recycled aggregate concrete made with iron ore tailings and polypropylene fibers. Journal of Building Engineering, 33, 101572. https://doi.org/10.1016/j.jobe.2020.101572
59. Young, G., Yang, M. 2019. Preparation and characterization of Portland cement clinker from iron ore tailings. Construction and Building Materials, 197, 152–156. https://doi.org/10.1016/j.conbuildmat.2018.11.236
60. Zhang, L. 2013. Production of bricks from waste materials–A review. Construction and building materials, 47, 643–655. https://doi.org/10.1016/j.conbuildmat.2013.05.043
61. Zhang, Y., Li, Z., Gu, X., Nehdi, M. L., Marani, A., Zhang, L. 2023. Utilization of iron ore tailings with high volume in green concrete. Journal of Building Engineering, 72, 106585. https://doi.org/10.1016/j.jobe.2023.106585
62. Zhao, J., Ni, K., Su, Y., Shi, Y. 2021. An evaluation of iron ore tailings characteristics and iron ore tailings concrete properties. Construction and Building Materials, 286, 122968. https://doi.org/10.1016/j.conbuildmat.2021.122968